Two Dimensional Metamaterial Slot Antenna for Improved Directivity

Student Name: Rohit Jain

IIIT-D M.Tech ECE

May , 2014

Indraprastha Institute of Information Technology

New Delhi

Thesis Committee

Submitted in partial fulfillment of the requirements

For the degree of M.Tech in Electronics and Communication Engineering

Certificate

This is to certify that the thesis titled "Two Dimensional Metamaterial Slot Antenna for improved directivity" submitted by Rohit Jain for the partial fulfillment of the requirements for the degree of Master of Technology in Electronics and Communication Engineering is a record of the bonafide work carried out by him under my guidance and supervision in the Electronics and Communication group at Indraprastha Institute of Information Technology, Delhi. This work has not been submitted anywhere else for the reward of any other degree.

Dr.Shobha Sundar Ram

Indraprastha Institute of Information Technology, New Delhi

Abstract

Directivity of an antenna is a figure of merit which shows how effective an antenna is at transmitting / receiving in a desired direction. A highly directive antenna is useful for applications such as satellite communications and radar systems. Directivity is usually achieved using either large antenna apertures or array systems comprising lots of antenna elements. More recently, metamaterials have been investigated for improving the directivity of different types of antennas such as linear wire antennas, patch antennas and horn antennas. Electromagnetic metamaterials are manmade materials which have unusual fundamental properties not readily available in nature. In this thesis, we investigate the possibility of improving the directivity of a slot antenna with a metamaterial substrate. We consider a two-dimensional metal waveguide with a slot and a metamaterial substrate with a point source excitation inside the substrate. The metamaterial substrate is modeled as a Debye medium with dispersive permittivity and permeability. The refractive index of the substrate is (a) negative at frequencies below the plasma frequency; (b) zero at the plasma frequency; and (c) positive at frequencies above the plasma frequency. Transverse magnetic mode wave propagation is simulated using finite difference time domain techniques with perfectly matched boundary conditions. Far field radiation patterns of the antenna are estimated from the electric field at the aperture of the slot. The effect of antenna parameters, such as the length of the aperture, the height of the substrate and the choice of the plasma frequency of the metamaterial, on the bandwidth and directivity of the antenna are studied. The results indicate that reduced beamwidth is achieved for a bandwidth of frequency around the plasma frequency when compared to a conventional slot antenna with an air substrate.

Acknowledgements

I am grateful to Dr.Shobha Sundar Ram for being an extraordinary advisor who was always there to guide me at difficult stages of research. Her enthusiasm, encouragement and faith in me throughout have been extremely helpful. I sincerely thank her for being my advisor for this period and for helping me positively with her vast knowledge.

I also thank IIIT Delhi for providing a enthusiastic and peace atmosphere, well facilitated computer labs to carry on work uninterrupted.

Rohit Jain

MT12102

Contents

List of Figures & Tables

Chapter 1: Introduction

Every communicating device whether it is a cellular phone, a Wi-Fi router, radio, television or large satellites uses antennas for transmitting and receiving signals. Highly directive antennas are required for those communication systems where point to point communication is necessary, for example satellite communication. The directivity of an antenna can be increased either by increasing the aperture size, as in dish antennas for television receivers, or with large synthetic aperture using an array of antennas. In this thesis, we wish to investigate the possibility of improving the antenna directivity without increasing the aperture size by using metamaterials. A brief overview and history of metamaterials is given in further sections.

1.1 What is a metamaterial?

As per Christophe Caloz and Tatsuo Itoh, electromagnetic metamaterials (MTMs) are broadly defined as "artificial effectively homogeneous electromagnetic structures with unusual properties not readily available in nature" [1]. Generally materials found in nature exhibit positive values of permittivity, ε and permeability constant, μ. Fig.1 shows materials with different combinations of permittivity and permeability and the nature of the resulting wave propagation within these mediums.

In 1967 Russian physicist Viktor Veselago [2] speculated the existence of a "substance with simultaneously negative values of ε and μ" depicted in III quadrant in Fig 1. He called these materials as left handed (LH) since these materials would allow the propagation of electromagnetic waves with the electric field, the magnetic field and the phase constant vectors satisfying a left-handed triad, compared with conventional materials where this triad is right handed i.e. the direction of propagation is opposite to that of direction of propagation in conventional materials. While different types metamaterials have been described in literature, in this thesis we will use metamaterials defined by the relative permittivity and permeability equations shown below.

$$\varepsilon = \varepsilon_0\left(1 - \frac{\omega_p^2}{\omega^2}\right) \tag{1}$$

$$\mu = \mu_0\left(1 - \frac{\omega_p^2}{\omega^2}\right) \tag{2}$$

Here, ω is frequency of source or excitation and ω_p is the plasma frequency of the metamaterial.

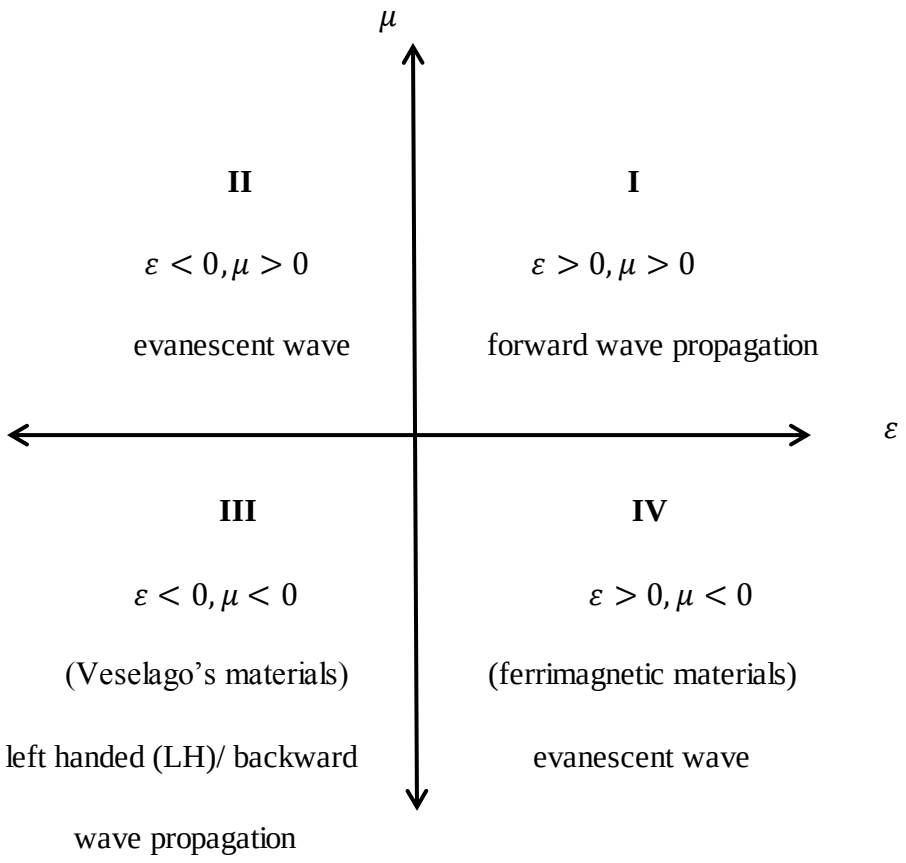

Fig 1 Different combinations of ε and μ and type of wave propagation in that medium.

1.2 History of metamaterials for antennas

In this section, we present a brief history of different investigations for improving antenna characteristics using metamaterials

In 2001 Ziolkowski [3] described how wave propagates in media having negative permittivity and permeability using finite difference time domain (FDTD) simulations. He explained that a perfect lens can be realized only for those frequencies where $\varepsilon(\omega) = \mu(\omega) = -1$. Therefore perfect lens behavior is only shown for $\omega=\omega_p/\sqrt{2}$ in (1). In Fig.2, the results of a two-dimensional (2-D) FDTD simulation are shown. The metamaterial region with a plasma frequency of 80GHz is defined within rectangular box and the source is kept along the line just

outside metamaterial region. The figure shows that the direction of the wave propagation changes inside the metamaterial when compared to free space outside the metamaterial.

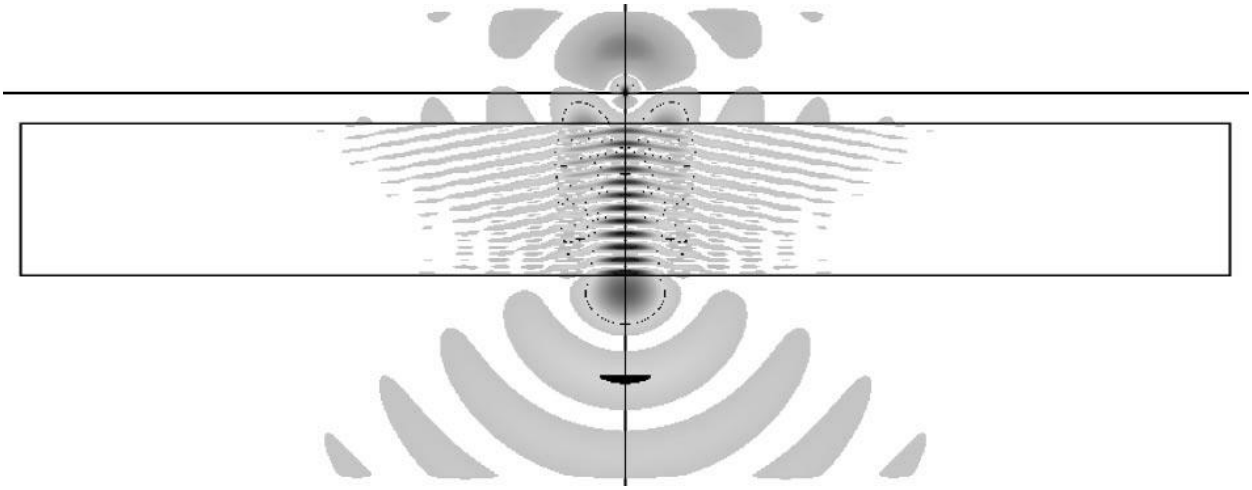

Fig: 2 2-D FDTD simulation of wave propagation in metamaterial. Note that the source is kept outside metamaterial. This figure is from [3].

In 2002, Enoch [4] showed how the unique characteristics of metamaterial defined by (1) can modify the emission of an embedded source as shown in Fig.3. The shaded region represents LH material while the un-shaded region represents free space. Note that the refractive index of the material is close to zero i.e. both ε and μ are zero when $\omega = \omega_p$. Using Snell's law of refraction, he showed that the rays are refracted in a direction close to normal, when $\omega = \omega_p$ (see Fig 3c). .

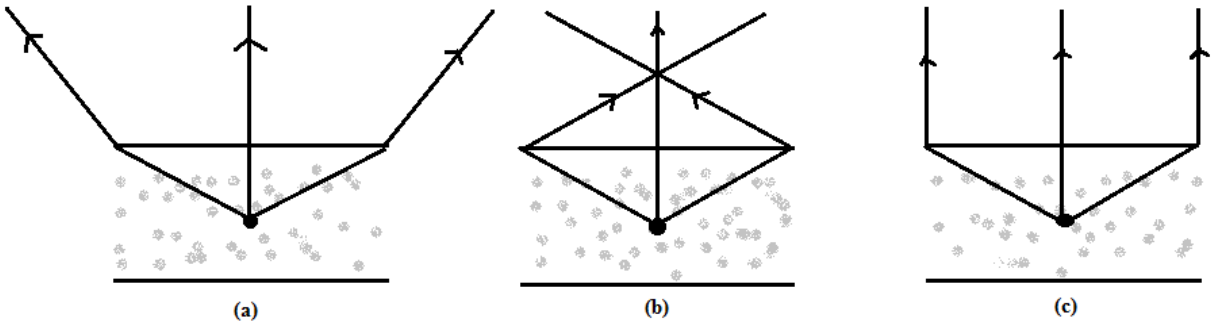

Fig 3) Different refraction scenarios when rays travel from metamaterial to free space. This figure is adapted from [4]

In the other two cases, when $\omega < \omega_p$ and when $\omega > \omega_p$ the rays either bend inwards or outwards respectively thereby decreasing the strength normal to interface. Therefore enhanced directivity can be realized when the refractive index of the material is near zero. Experimental verification of Enoch's results was carried out by Zhou [5] in 2010. He embedded a monopole within a linear wire array as shown in Fig.4. The wire array was designed such that the effective refractive index of the medium constituted by the array was close to zero at some frequency. His results showed improved directivity of the monopole for that frequency.

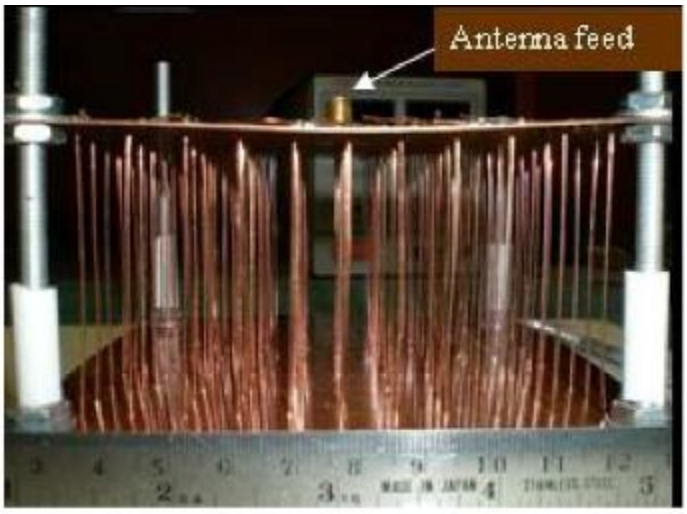

Fig 4) A photo of the fabricated antenna prototype.taken from [5]..

Hongkiang Li in 2004 [6], came up with a directive metamaterial antenna using a high impedance surface (HIS). He showed that a metamaterial cavity formed by HIS and an electrically responded surface makes a dipole highly directive.

Zi bin Wang in 2006 [7], proposed a high gain patch antenna with a metamaterial cover. At 2.55 GHz, the gain of the metamaterial patch antenna was found to be 2.5 times greater than the gain of a conventional patch antenna. Reduction in half power beam width was also achieved

In 2009, Soon Ho Hwang [8], proposed a design for an antenna based on composite right/left handed (CRLH) metamaterial, for a mobile hand set application. A broad bandwidth antenna covering variety of commercial bands such as Bluetooth, wimax, etc. was proposed.

Mohamed Lashab in 2011 [9] proposed a horn antenna (see Fig 5) loaded by a metamaterial substrate for terrestrial digital video broadcast (DVB-T) applications. The horn operated between 0.5 GHz and 1.2 GHz. The metamaterial was a low indexed type rather than DNG. Fig 5 shows the designed horn antenna.

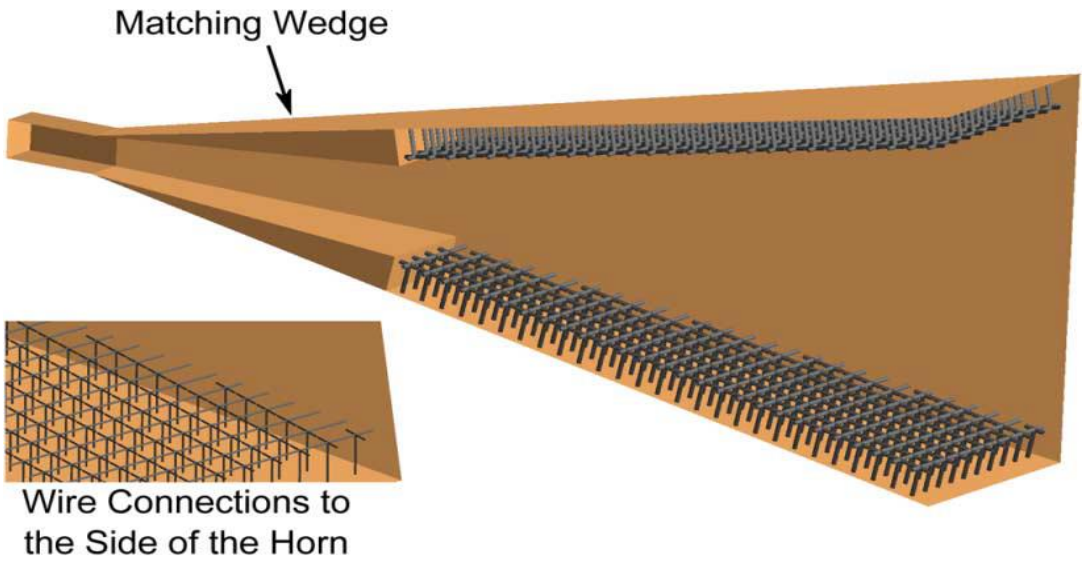

Fig.5 Horn antenna with wire grid for achieving directivity taken from [9]

Yue-Long-Lv in 2013 [10] used metamateial for enhancing gain of a patch antenna. Clinton P. Scarborough in 2013 [11] proposed a metamaterial horn antenna for satellite with a very high directivity.

1.3 Problem Statement and Objectives

In this thesis we propose to investigate the use of a double negative substrate for improving the directivity of a slot antenna. Slot antennas are very popular because of their low profiles, ease of fabrication and frequency scanning capabilities. We use computational electromagnetic techniques for studying the wave propagation mechanisms in the simulated antenna structure. Correa and Jin [12] in 2003 came up with theoretical analysis of left handed metamaterials using FDTD-PML method. Ziolkowski, [13] highlighted the advantage of a purely numerical simulation approach to study pulsed and continuous wave Gaussian beam interactions with DNG

slabs. In our case, we consider a broadband source embedded inside a two dimensional waveguide with a slot and a DNG substrate. The time-domain electric and magnetic fields in this antenna are simulated with FDTD simulations. Z-transform techniques, originally proposed by Sullivan [14], are used for modeling the dispersive nature of permittivity and permeability of the substrate. The far field radiation characteristics of our antenna are studied using field equivalence principles.

The thesis report is organized as follows. We have started by introducing metamaterials in chapter 1. This is followed by describing the motivation for slot antenna design with double negative substrate for high directivity. Then a brief history of various works in metamaterial antenna applications is described. In chapter 2 the problem statement is described in detail with the proposed mathematical modeling. Chapter 3 highlights important results and inferences. Conclusion and future work are presented in chapter 4.

Chapter 2: Problem Statement and Modeling

In this chapter, we investigate the directivity of a two-dimensional slot antenna with a metamaterial substrate. The problem space is modeled as a 1.125m × 1.125 m space in the X-Y Cartesian coordinate space as shown in Fig.6. We consider a waveguide of thickness *h*, with perfect electric conductor (PEC) walls. The region inside the waveguide is metamaterial with dispersive permeability and permittivity as shown below,

$$\mu = \mu_0\left(1 - \frac{\omega_p^2}{\omega^2}\right)$$

$$\varepsilon = \varepsilon_0\left(1 - \frac{\omega_p^2}{\omega^2}\right) \quad (3)$$

where ω is the source frequency and ω_p is the plasma frequency of the metamaterial. Note that the permeability and permittivity are negative for frequencies lower than the plasma frequency of the substrate. The region outside the waveguide is free space with $\varepsilon = \varepsilon_0$ and $\mu = \mu_0$. A slot aperture of length SL is introduced in the waveguide. The problem is modeled using 2D finite difference time domain (FDTD) technique in MATLAB 2013b.

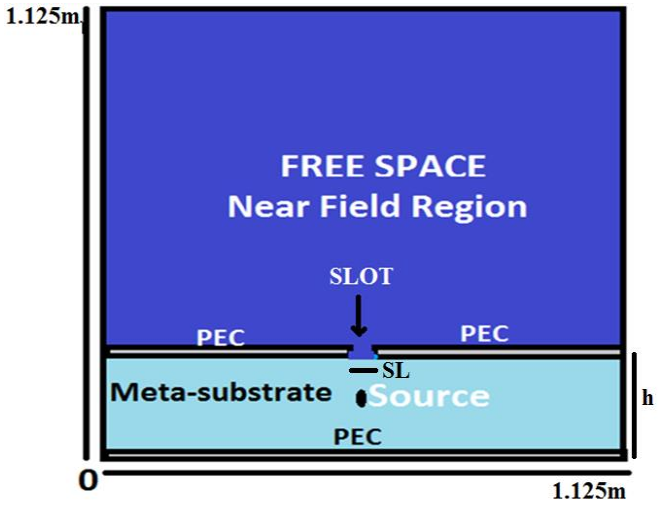

Fig (6) Problem space diagram

A perfectly matched layer (PML) for free space is implemented at the boundaries of the problem space [14][16]. Note that this PML is equally suited for the region with the metamaterial

substrate since the intrinsic impedance, η, of the metamaterial region is equal to that of free space

$$\eta = \sqrt{\frac{\mu_0}{\varepsilon_0}} = \eta_{\text{free space}} \tag{4}$$

A Gaussian pulse with a pulse width of 0.25 ns is used as the excitation source. Thus the frequency domain response is considered up to 2 GHz. Fig 7 shows the dispersive permittivity for three different plasma frequencies. Note that when $\omega < \omega_p$, the refractive index becomes negative for the medium, which therefore shows left handed (LH) properties. Also, higher value of ω_p implies that most of the frequency components exist in the negative permittivity region.

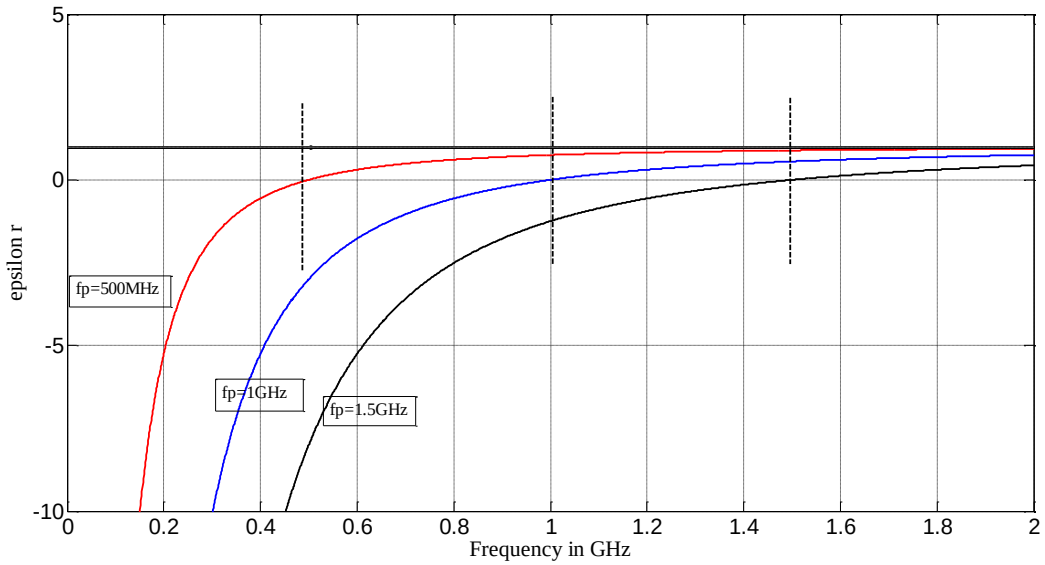

Figure 7 ε_r vs. frequency plot for metamaterial substrate

2.1 Derivation of two dimensional (2D)-FDTD equations -

For deriving the 2D-FDTD equations for wave propagation with frequency dependent permittivity and permeability values, we start with Maxwell's equation for electric and magnetic fields as shown in (5) and (6).

$$\nabla \times \vec{E} = -\partial \vec{B} / \partial t \tag{5}$$

$$\nabla \times \vec{H} = \sigma\vec{E} + \partial\vec{D}/\,\partial t \tag{6}$$

where $\vec{E}$ is electric field intensity, $\vec{H}$ is magnetic field intensity, $\vec{B}$ is magnetic flux density and $\vec{D}$ is electric flux density. We consider TM mode of propagation with E_z, H_x and H_y components. We use equations (3) for ε and μ. In order to model the PEC walls, ε is modified to include the effect of conductivity. Therefore, the phasor relation between $\vec{D}$ and $\vec{E}$, is given by

$$D_z(\omega) = \varepsilon_0\left(1 - \frac{\omega_p^2}{\omega^2} + \frac{\sigma}{j\omega\varepsilon_0}\right) E_z(\omega) \tag{7}$$

where σ is conductivity, D_z and E_z are components of $\vec{D}$ and $\vec{E}$ in z direction. We model the dispersive nature of permittivity using z-transform techniques proposed by Sullivan [14]. The frequency domain relation in (7) is converted to z-domain using transformation shown in (8),

$$j\omega \rightarrow \frac{1-z^{-1}}{\Delta t} \tag{8}$$

where Δt is the time step defined in the FDTD simulation. Therefore, by substituting value of jω term as given in (8) into (7), it reduces to

$$D_z(z) = \varepsilon_0 E_z(z) + \varepsilon_0 \frac{\omega_p^2 \Delta t^2}{(1-z^{-1})^2} E_z(z) + \frac{\sigma\Delta t}{1-z^{-1}} E_z(z) \tag{9}$$

This is further broken into intermediate terms, I_{1z} and I_{2z}, to make manipulations and programming easier as

$$I_{1z} = \varepsilon_0 \frac{\omega_p^2 \Delta t^2}{(1-z^{-1})^2} E_z(z) \tag{10}$$

$$I_{2z} = \frac{\sigma\Delta t}{1-z^{-1}} E_z(z) \tag{11}$$

Further simplifying these equations and then taking inverse z transform gets us to the discrete time domain equations, which are then coded in MATLAB.

$$I_{1z}(n) = \varepsilon_0\omega_p^2\Delta t^2 E_z(n) - I_{1z}(n-2) + 2I_{1z}(n-1)$$

$$I_{2z}(n) = I_{2z}(n-1) + \sigma\Delta t E_z(n)$$

$$E_z(i,j,n) = \frac{D_z(i,j,n) - 2I_{1z}(i,j,n-1) + I_{1z}(i,j,n-2) - I_{2z}(i,j,n-1)}{\varepsilon_0\left(1 + \omega_p^2\Delta t^2 + \frac{\sigma\Delta t}{\varepsilon_0}\right)} \tag{12}$$

The magnetic flux density, $\vec{B}$, is related to magnetic field intensity, $\vec{H}$, through the equation

$$B_x(\omega)\hat{\imath} + B_y(\omega)\hat{\jmath} = \mu_0\left(1 - \frac{\omega_p^2}{\omega^2}\right)(H_x\hat{\imath} + H_y\hat{\jmath})$$

where B_x and B_y are x and y components of $\vec{B}$ respectively. We use similar methods to solve for H_x and H_y and get the equations shown in (13).

$$I_{1x}(n) = \mu_0\omega_p^2\Delta t^2 H_x(n) - I_{1x}(n-2) + 2I_{1x}(n-1)$$

$$H_x(i,j,n+1) = \frac{B_x(i,j,n+1) - 2I_{1x}(i,j,n) + I_{1x}(i,j,n-1) - I_{2x}(i,j,n)}{\mu_0(1+\omega_p^2\Delta t^2)}$$

$$I_{1y}(n) = \mu_0\omega_p^2\Delta t^2 H_y(n) - I_{1y}(n-2) + 2I_{1y}(n-1)$$

$$H_y(i,j,n+1) = \frac{B_y(i,j,n+1) - 2I_{1y}(i,j,n) + I_{1y}(i,j,n-1) - I_{2y}(i,j,n)}{\mu_0(1+\omega_p^2\Delta t^2)} \quad (13)$$

The electric field and magnetic field equations defined in (12) and (13) respectively are implemented in leap frog equations traditional to FDTD simulations. A Gaussian pulse excitation of pulse width = 0.25ns is placed inside the metamaterial substrate and the FDTD simulations are carried out for a duration of 5800 steps.

2.2) Derivation of far field equations from near field equations -

The FDTD simulation enables us to calculate the time domain near field values within the problem space. Using Fourier transform, we calculate the frequency domain near field values. To calculate the directivity, analysis must be done in far field. In order to estimate the far field electric field from near field values, vector potentials are first calculated from source current densities

The tangential electric field along the PEC is zero but not-zero in the slot aperture. This implies that the boundary conditions along the slot interface can be modeled as a non-zero magnetic surface current density, $\overrightarrow{M_s}$, along the aperture. Using field equivalence principles, $\overrightarrow{M_s}$ is given by

$$\overrightarrow{M_s} = 2\overrightarrow{E_a} \times \hat{n} \quad (14)$$

where $\hat{n}$ is the unit vector perpendicular to the surface. $\overrightarrow{E_a}$ is the phasor electric field computed through Fourier transform of the time domain aperture field obtained through FDTD, hence

$$\overrightarrow{M_s} = -2E_a\hat{x} \tag{15}$$

The electric vector potential, $\vec{F}$ is related to $\overrightarrow{M_s}$ through

$$\vec{F}(r) = \frac{1}{4\pi}\int \overrightarrow{M_s}(r')\frac{e^{-jk|\vec{r}-\vec{r'}|}}{|\vec{r}-\vec{r'}|}dl \tag{16}$$

where $\left|\vec{r}-\vec{r'}\right|$ is used to compute the far field component.

$$\left|\vec{r}-\vec{r'}\right| = \sqrt{(x-x')^2+(y-y')^2} \tag{17}$$

The primed parameters indicate source (along the aperture) while the unprimed parameters are the scattered field (see Fig 8)

The E field in the far field is obtained by: $\vec{E} = \overrightarrow{\nabla_r}\times\vec{F}$

Putting (16) and (17) together gives

$$\vec{E} = \frac{1}{4\pi}\overrightarrow{\nabla_r}\times\int \overrightarrow{M_s}(r')\frac{e^{-jk|\vec{R}|}}{|\vec{R}|}dl$$

where $|\vec{R}|=\left|\vec{r}-\vec{r'}\right|$ and dl is unit length in the aperture

Further simplifying leads to

$$\vec{E} = \frac{-1}{4\pi}\int(\overrightarrow{M_s}(r')\times\hat{r})(jk+\frac{1}{|\vec{R}|})\frac{e^{-jk|\vec{R}|}}{|\vec{R}|}dl \tag{18}$$

Now, field at aperture is due to z-polarized plane wave and direction normal to aperture is y direction. We use $jk = \frac{j\omega}{c_o}$ and ignore the $\frac{1}{R^2}$ terms due to far field considerations. Therefore (18) reduces to

$$\overrightarrow{E_f}(x,y,\omega) = \frac{1}{2\pi}\sum_{i=ap\_i}^{ap\_f} r_y\vec{E}_{ai}(x',y',\omega)(jk)(\frac{e^{-jk|\vec{R}|}}{|\vec{R}|})\Delta l \tag{19}$$

where, (see Fig 8)

ap_i = initial aperture position co-ordinate

ap_f = final aperture position co-ordinate

$\overrightarrow{E_{ai}}$= Electric field at aperture position i

Δl = length of one cell

r_y= component of $\vec{R}$ in y direction

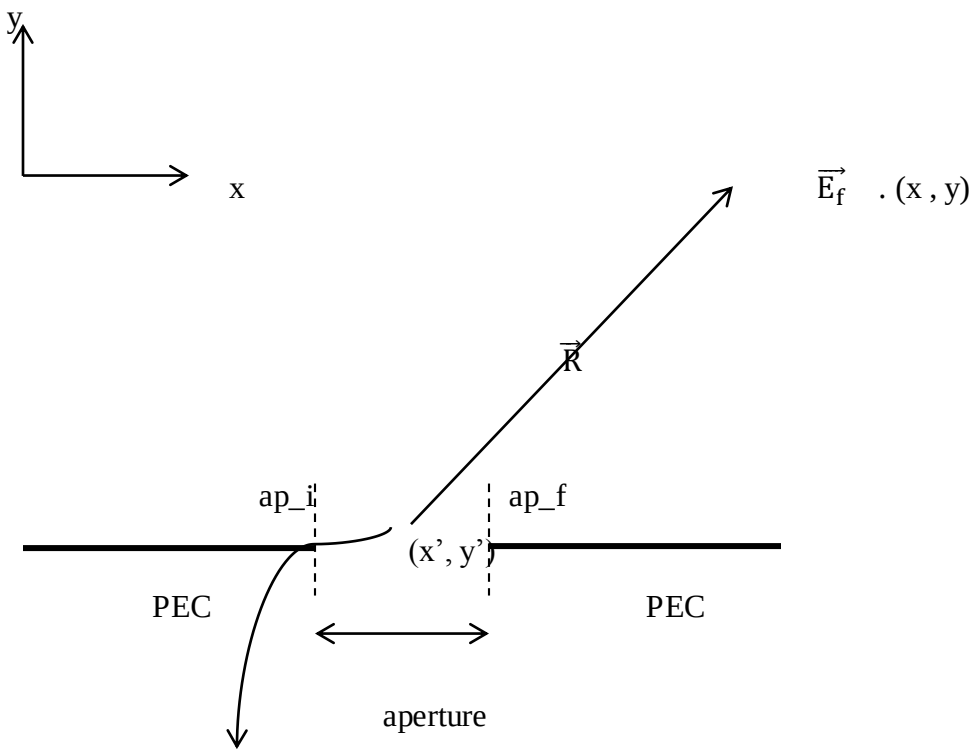

$\overrightarrow{E_a}$, electric field at aperture

Fig 8: Pictorial explanation of important variables and constants used in equations

Chapter 3: Results

In this chapter we compare the performance of the proposed 'slot antenna with metamaterial substrate' with the performance of a 'conventional slot antenna with an air substrate'. We also study the effect of the following parameters on the antenna characteristics:

(a) The plasma frequency, f_p

(b) The slot length (SL) in terms of wavelength corresponding to plasma frequency λ_p

(c) The thickness of the substrate (h) in terms of λ_p

For each case, we study the radiation characteristics of the antenna as a function of the parameter, the beam width of the antenna as a function of operation frequency, and the signal strength at far field at a position normal to the aperture as a function of operation frequency.

Case (I)

The overall improvement due to a metamaterial substrate with f_p=1 GHz, thickness h=0.3 m, and slot length, SL=0.6m, is compared with a similar dimension antenna structure without metamaterial in Fig.9. Using the techniques described in the previous chapter, we compute the radiation patterns. The far field pattern plot in Fig.9(a) was calculated for a radial distance of 100m along the azimuth plane. We observe that the directivity of the slot antenna with the metamaterial substrate is superior to the slot antenna with the air substrate. Next, we compare the beam widths of the two antennas as a function of the excitation frequency in Fig.9b. We note that there is a significant improvement in directivity for a bandwidth of frequencies around $\omega = \omega_p$ ($\omega_p = 2\pi f_p$) when compared to the conventional slot. Also f_p(1GHz) is the geometric mean of the upper (1.43GHz) and lower frequencies (0.7GHz) of this bandwidth. Fig.9c shows the absolute field strength at a point that is 100 m from the center of the aperture at an azimuth angle of 90^o. We observe that the absolute field strength is increased in the bandwidth of frequencies around $\omega = \omega_p$.

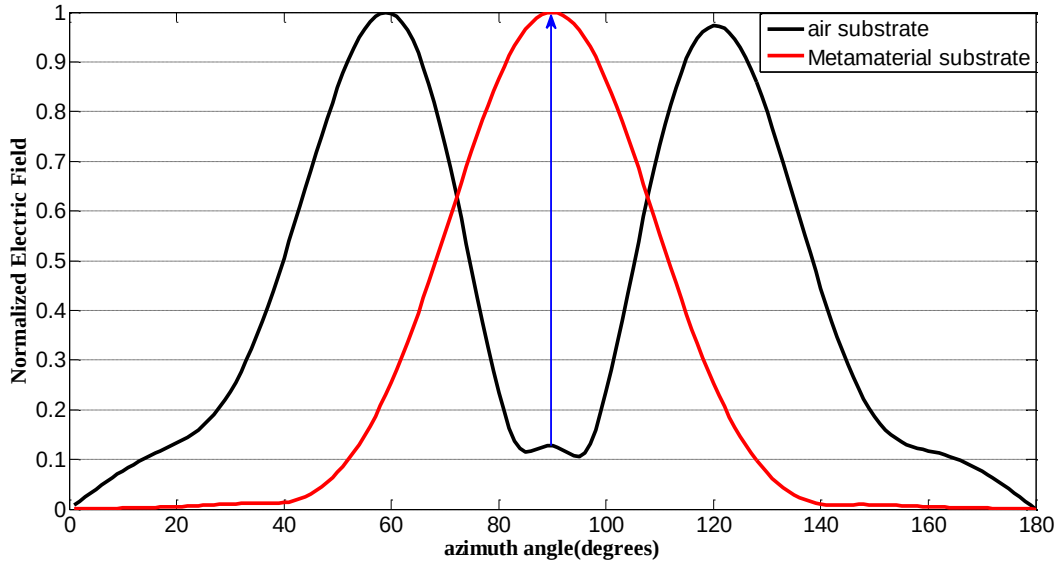

Figure 9(a) Normalized far field radiation pattern comparing metamaterial substrate slot antenna with air substrate antenna, for: f_p =1GHz, SL=2λ_p, h= λ_p.

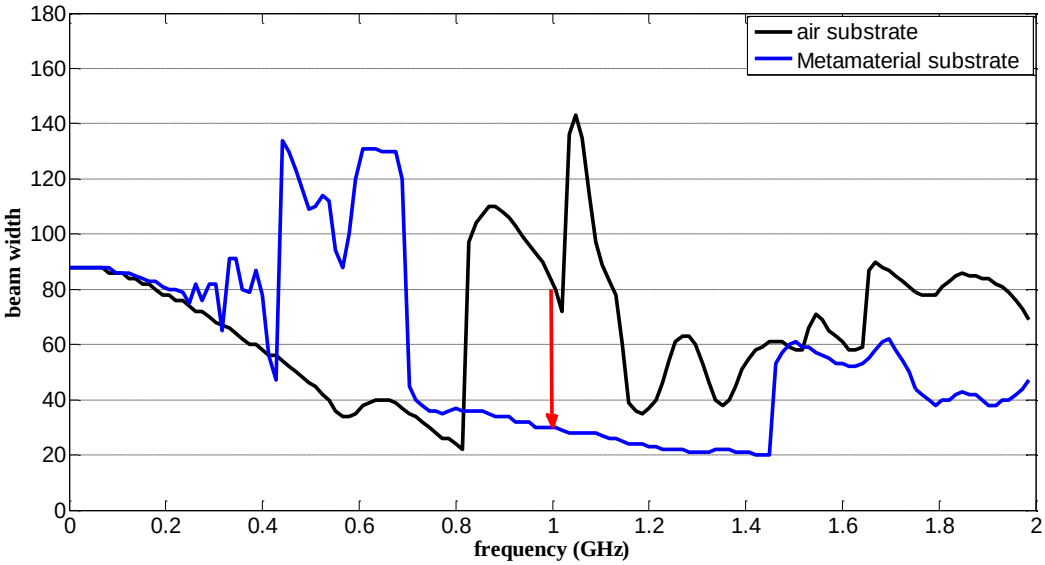

Figure 9(b) Beam width vs. frequency plot for comparing air substrate slot antenna with metamaterial substrate slot antenna, for : f_p =1GHz, SL=2λ_p, h= λ_p.

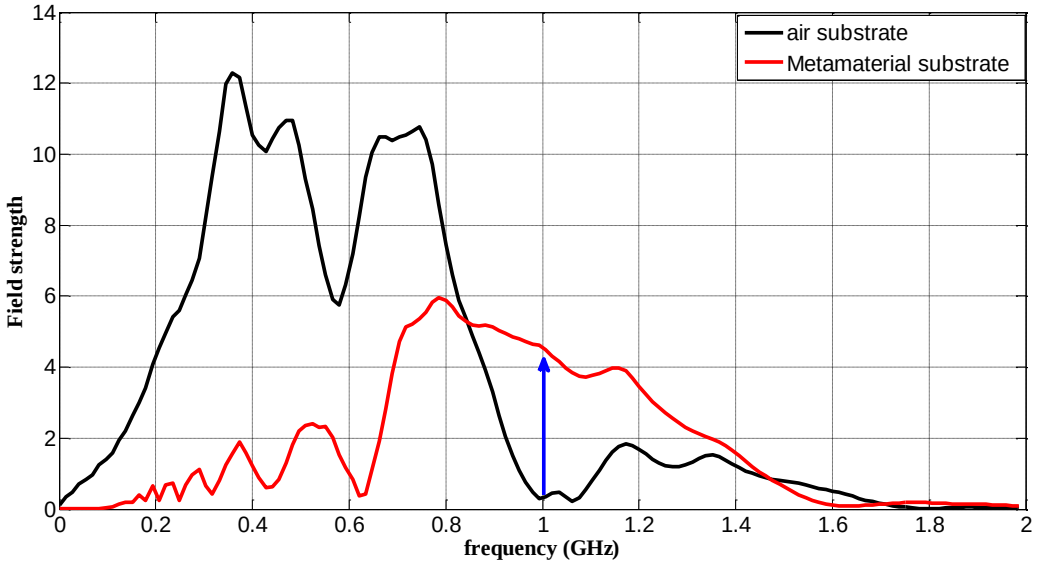

Figure 9(c) Absolute far field strength at $\varphi = 90^{o}$ vs. for an air substrate slot antenna and metamaterial substrate slot antenna, for f_p =1GHz, SL=2λ_p, h= λ_p

Case (II)

Next, the length of the slot is varied while f_p is constant (1 GHz) and thickness of substrate is 0.3 m. We observe that the directivity improves with increase in slot length in Fig.10a. The reduction in beam width is more when L is changed from 1 to 2 where L is the ratio of slot length and λ_p.

$$L = \frac{SL}{\lambda_p} \tag{20}$$

When we increase SL from $2\lambda_p$ to $3\lambda_p$, the reduction in beam width is less. Fig 10(b) shows an interesting tradeoff between bandwidth and directivity. The figure also shows that for smaller slot length metamaterial behavior is not dominant. Fig.10(c) shows that SL=2 λ_p is a good choice as strength for L=2 and L=3 are higher.

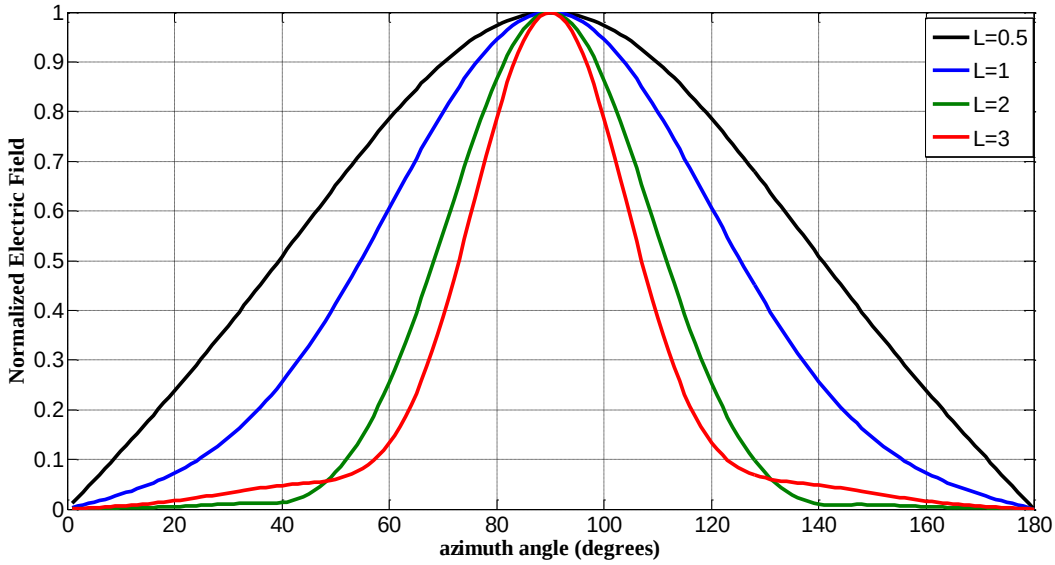

Figure 10(a) Normalized far field pattern plot for a metamaterial slot antenna with different slot lengths, other constant values are: f_p =1GHz, SL=0.5λ_p, λ_p, 2λ_p, 3λ_p, h= λ_p.

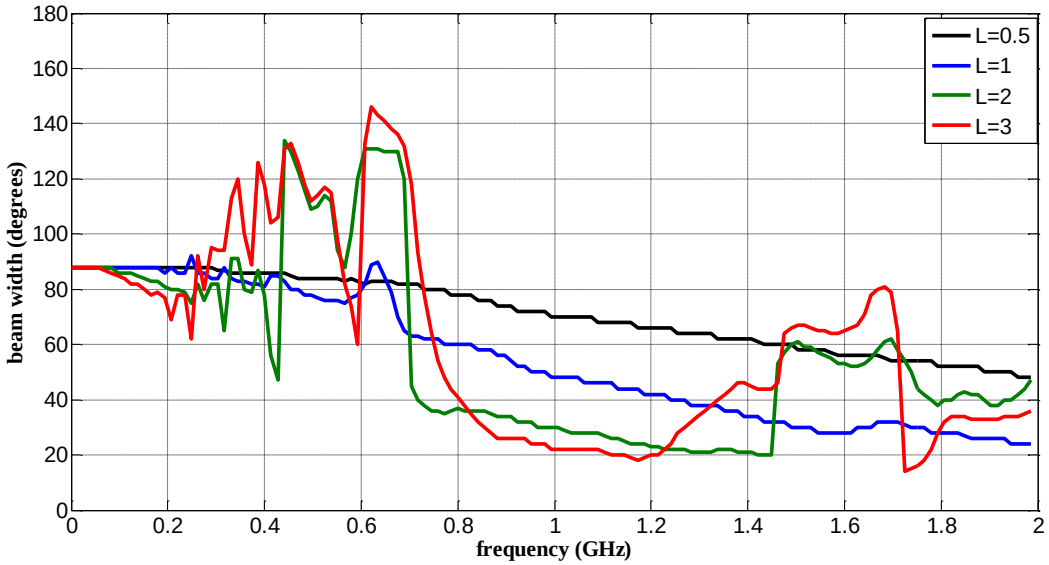

Figure 10 (b) Beam width vs. frequency plot for a metamaterial slot antenna with different slot lengths, other constant values are: f_p =1GHz, SL=0.5λ_p, λ_p, 2λ_p, 3λ_p, h= λ_p.

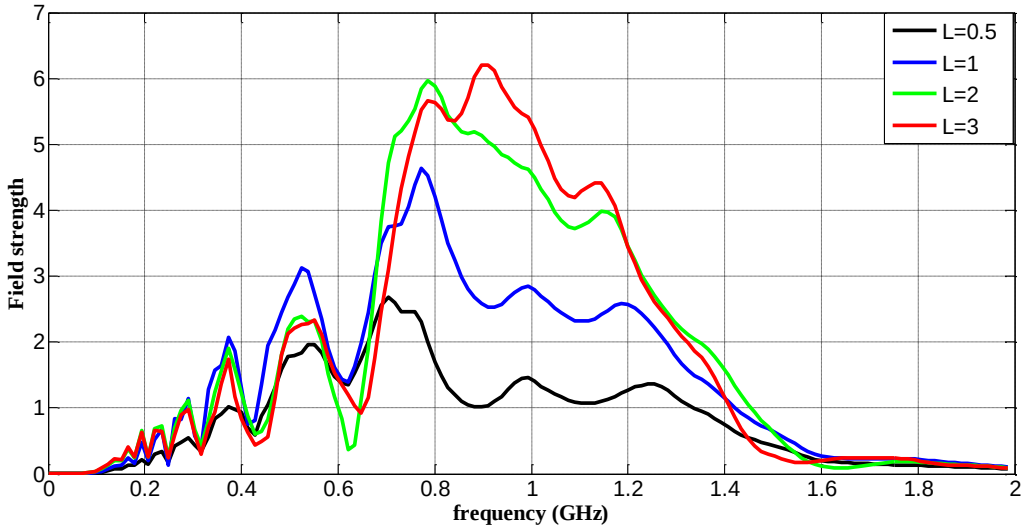

Figure 10 (c) Absolute far field strength at φ = 90° vs. frequency plot for a metamaterial slot antenna with different slot lengths, where f_p =1GHz, SL=$0.5\lambda_p, \lambda_p, 2\lambda_p, 3\lambda_p$,h= λ_p.

Case (III)

Next, we analyze the effect of variation in thickness while keeping other two parameters constant: f_p is kept as 1 GHz and length of slot, SL as $2\lambda_p$. This slot length is selected due to reasons explained in case II. From the far field pattern plot in Fig.11(a) and beam width plot in Fig.11(b), we observe that the directivity improves with thickness but it seems to quickly converge as T increases. Here,

$$T=\frac{h}{\lambda_p} \qquad (21)$$

Fig.11(b) shows that although there is not much improvement in beam width with increase in thickness of substrate, the bandwidth of frequencies with lower beamwidths increases with thickness of substrate. Fig.11(c) shows the magnitude of electric field as a function of frequency for φ = 90°. We observe that the field strength decreases for higher thickness.

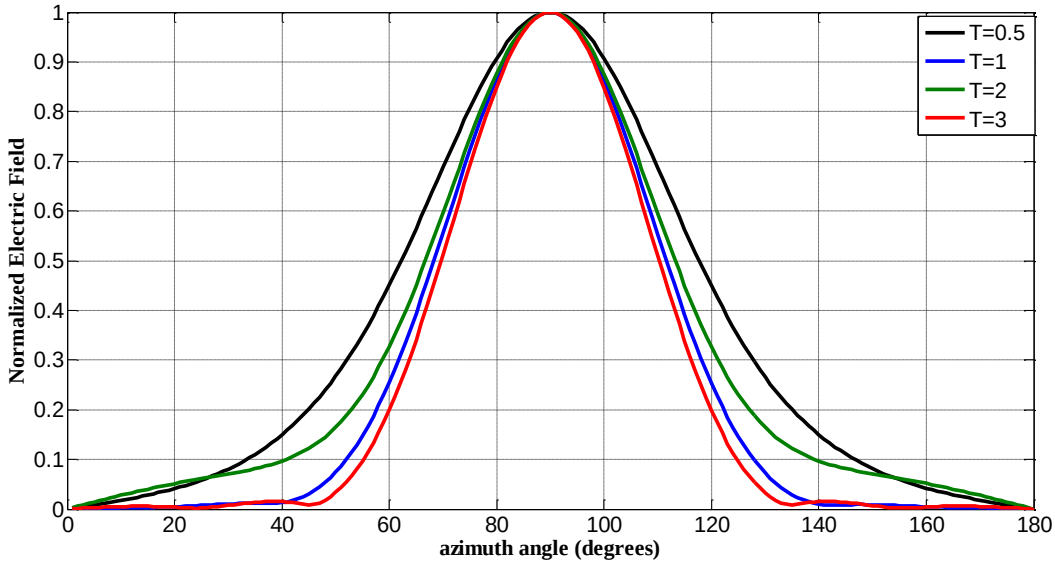

Figure 11(a) Normalized far field pattern plot for a metamaterial slot antenna with different substrate thickness, other constant values are: f_p =1GHz, SL=2 λ_p ,h=$0.5\lambda_p, \lambda_p, 2\lambda_p, 3\lambda_p$.

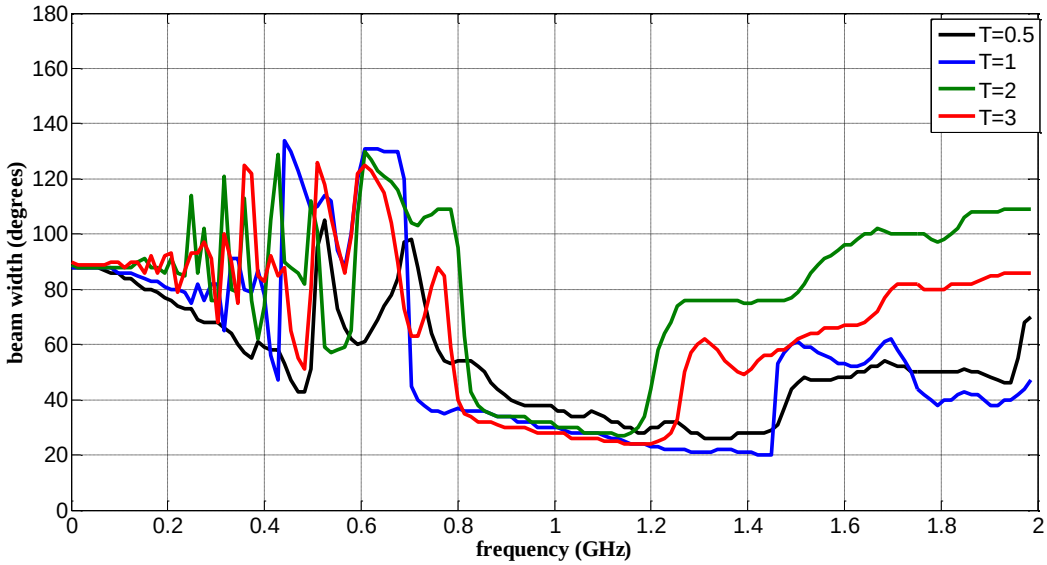

Figure 11(b) Beam width vs. frequency plot for a metamaterial slot antenna with different substrate thickness, other constant values are : f_p =1GHz, SL=2 λ_p ,h=$0.5\lambda_p, \lambda_p, 2\lambda_p, 3\lambda_p$.

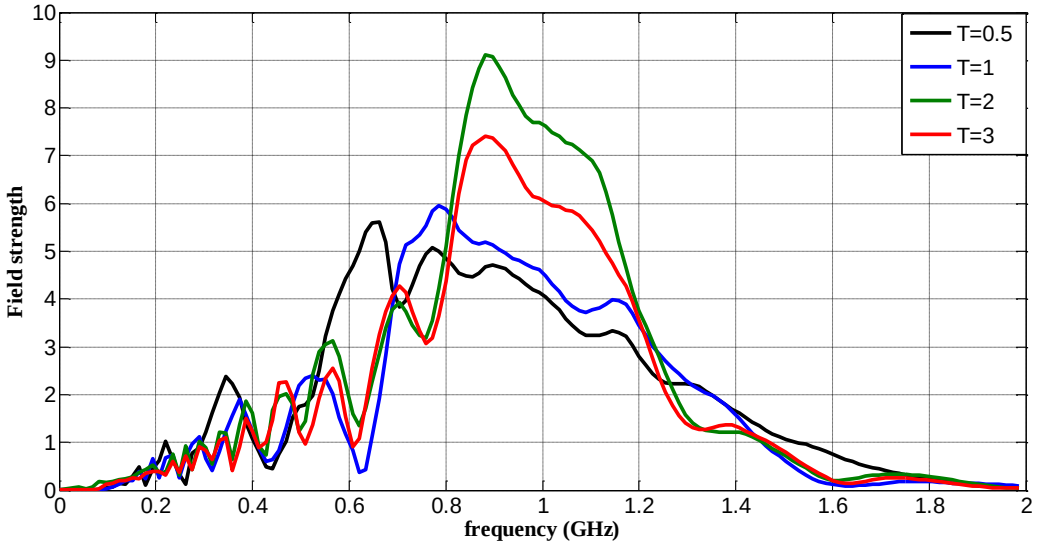

Figure 11(c) Absolute far field strength at $\varphi = 90^{o}$ vs. frequency plot for a metamaterial slot antenna with different substrate thickness, other constant values are: f_p =1GHz, SL=2 λ_p ,h=$0.5\lambda_p, \lambda_p, 2\lambda_p, 3\lambda_p$.

Case (IV)

Next, we consider different plasma frequencies while keeping the slot length and thickness of substrate constant: L=2 and T=1. It is observed in Fig 12(a) that the directivity results are almost the same for metamaterials with different plasma frequencies. But Fig 12(b) shows an interesting result that although beam width is in same range for different choices of ω_p, the bandwidth changes at the cost of field strength (Fig.12(c))..

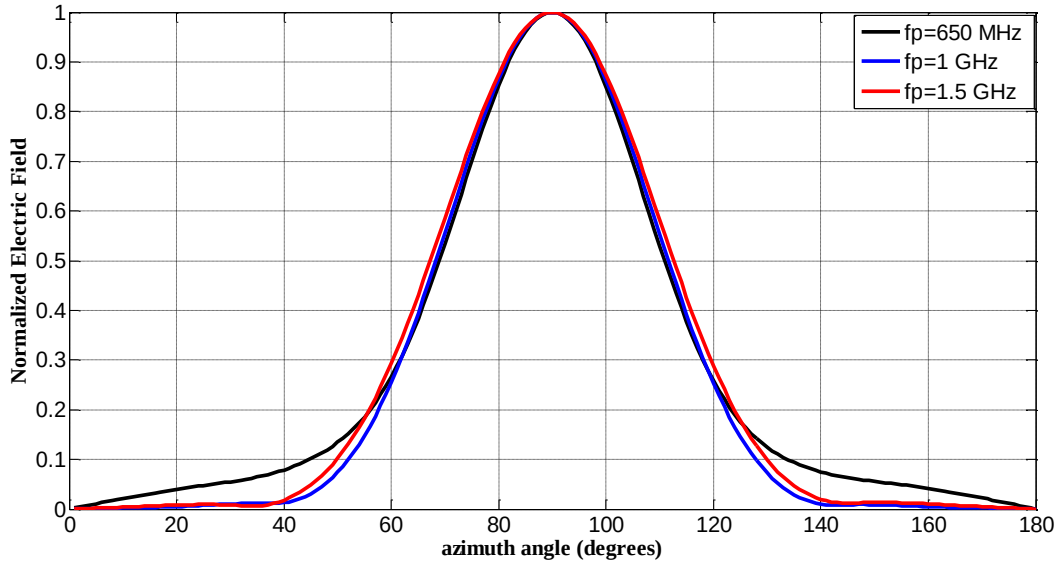

Figure 12(a) Normalized far field pattern plot for different plasma frequency metamaterial slot antenna, other constant values are: f_p =640 MHz, 1GHz, 1.5 GHz, SL=$2\lambda_p$, h=λ_p.

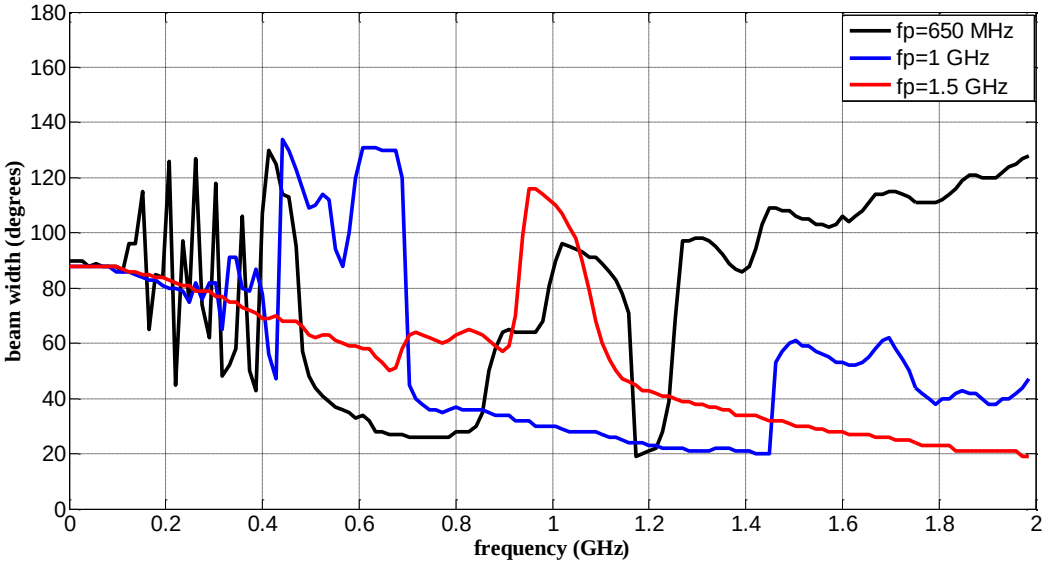

Figure 12(b) Beam width vs. frequency plot for different plasma frequency metamaterial slot antenna, other constant values are:f_p =640 MHz, 1GHz, 1.5 GHz, SL=$2\lambda_p$, h=λ_p.

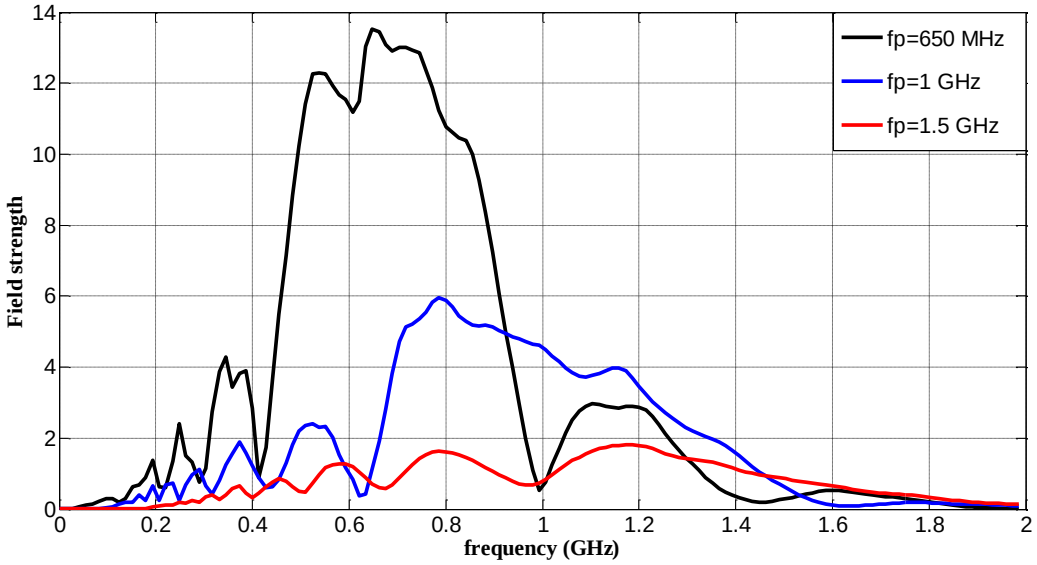

Figure 12(c) Absolute far field strength at φ = 90° vs. frequency plot for different plasma frequency metamaterial slot antenna, other constant values are: f_p =640 MHz, 1GHz, 1.5 GHz, SL=$2\lambda_p$, h=λ_p.

Case (V)

In this case, we consider the proposed slot with the parameter values that resulted in optimum bandwidth and directivity from the above cases. Therefore, f_p=1GHz, SL=$2\lambda_p$ and h=λ_p. We consider the far field radiation patterns for different source frequencies as shown in Fig.13(a). We observe that for $\omega = \omega_p$ the pattern has the lowest half power beam width (HPBW). Then we consider the beam width as a function of source frequencies ranging up to 2 GHz as shown in Fig.13(b). The low beam widths are obtained for a bandwidth (750MHz) of frequencies around $f = f_p$. Interestingly, the f_p is the geometric mean of upper and lower frequencies of this bandwidth. The absolute far field strength at φ = 90° is shown in Fig.13(c) where we notice that the field strength is maximum at 80 MHz. This is close to the frequency at which $\varepsilon(\omega) = \mu(\omega) = -1$ and it occurs at $\omega=\omega_p/\sqrt{2}$. This result is consistent with the perfect lens case that was presented earlier in [4].

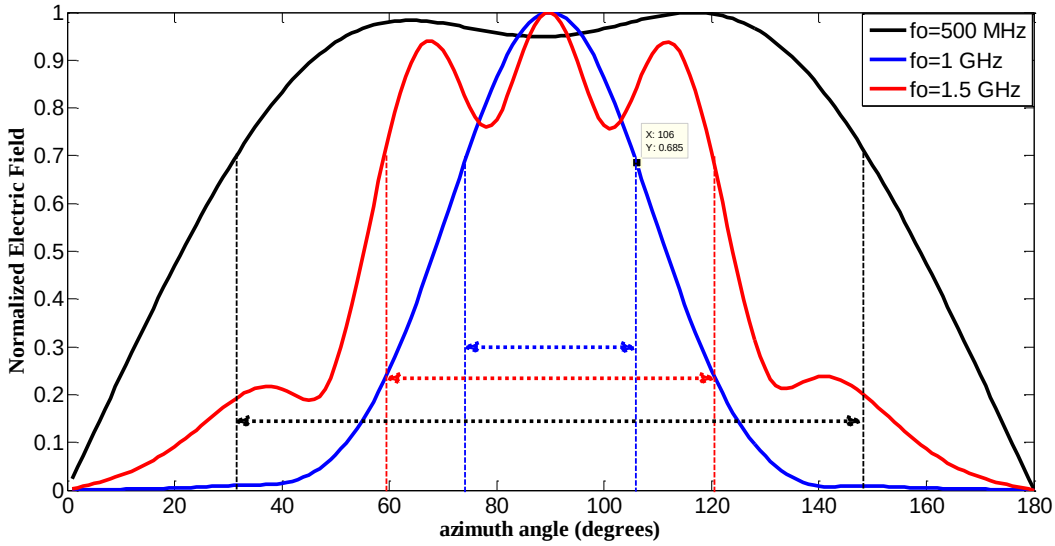

Figure 13(a) Normalized far field pattern plot for metamaterial slot antenna with parameter values as : f_p =1GHz,SL=2 λ_p ,h=λ_p. HPBW is shown with horizontal dotted lines.

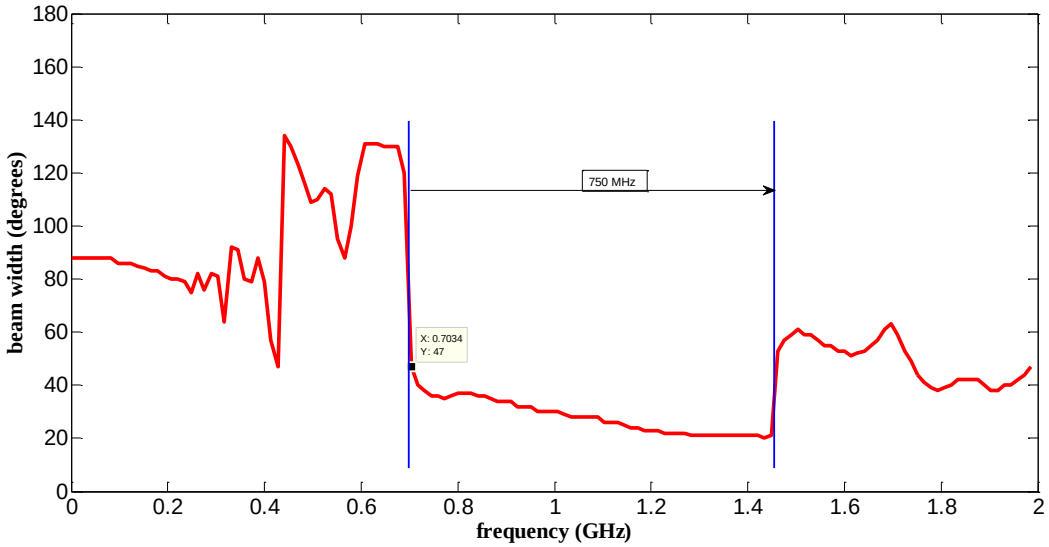

Figure 13(b) Beam width at different frequencies for metamaterial slot antenna with parameter values as f_p =1GHz, SL=2λ_p, h=λ_p.

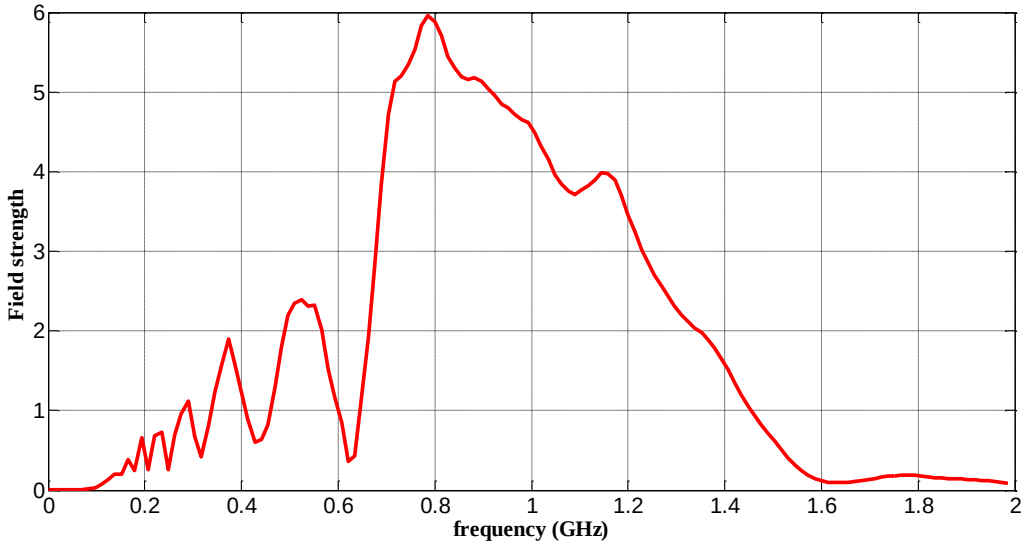

Figure 13(c) Absolute field strength plot for metamaterial slot antenna with parameter values as: f_p =1GHz, SL=2λ_p, h=λ_p,

The summary of our studies are presented in the table below.

Case	**Plasma frequency, f_p**	**Slot length, SL**	**Thickness, h**	**Inferences**
Case 1	1GHz compared with no substrate slot antenna	$2\lambda_p$	λ_p	a. Improvement in beam width by 50˚ b. Field strength is also improved for a bandwidth of frequency
Case 2	1 GHz	varying	λ_p	a. Low beam width for L=2 & 3 but almost same. b. Tradeoff between beam width and bandwidth
Case 3	1 GHz	$2\lambda_p$	varying	a. Beam width converges for T=1 and T=3 b. Higher bandwidth for T=1 c. Field strength is more for T=1
Case 4	Varying	$2\lambda_p$	λ_p	a. With change in ω_p beam width is almost unaffected. b. Bandwidth increases with ω_p but at cost of field strength.
Case 5	1 GHz	$2\lambda_p$	λ_p	a. Least beam width at $\omega = \omega_p$ b. Side lobes shows for frequencies out of bandwidth.

Table 1 Result analysis case wise

Chapter 4: Conclusion and Future Work

A two dimensional slot antenna with a metamaterial substrate is successfully simulated using FDTD techniques and the far field radiation patterns are generated. The behavior of the antenna for different parameters such as the length of the slot, the height of the substrate and the plasma frequency of the substrate, is analyzed. These were our key findings:

1. The directivity of the slotted antenna with a metamaterial substrate was found to substantially improve upon the directivity of a conventional slot antenna with air substrate. Furthermore, the improved directivity was achieved for a bandwidth of frequencies around the plasma frequency.
2. As the size of the aperture increases, the directivity of the antenna also increases till it converges. However, there is a tradeoff between beam width and bandwidth
3. Similarly, as the height of the substrate increases, the directivity increases till it reaches convergence.
4. The choice of the plasma frequency of the metamaterial impacts the bandwidth considerably but not the beam width of the antenna.

FUTURE WORK-

1. While we have analyzed the radiation behavior of a single slot element, our study could easily be extended to a slotted antenna array with a metamaterial substrate along the lines of a leaky wave antenna. Array parameters such as spacing between the elements, differential phasing of the elements etc. can be studied to further improve the performance of the antenna.
2. The two dimensional modeling that was considered in this thesis can be modified to complete three-dimensional modeling, which will result in a more realistic simulation of practical antenna implementations

Finally, we must validate our proposed antenna design with measurement data collection with an actual hardware implementation. The plasma behavior of the substrate can be achieved with split ring resonators.

Bibliography

[1] C. Caloz and T Itoh, (2005, November). '*Electromagnetic metamaterials: transmission line theory and microwave applications'*. Wiley and IEEE Press. p. 376.

[2] V. Veselago Sov, 'The electrodynamics of substances with simultaneously negative values of ε and μ'. *Sov. Phys. Usp*. 10 (4): 509–14, 1966.

[3] R. Ziolowski, 'Wave propagation in media having negative permittivity and permeability', *Physical Review Letter*, 2001.

[4] S. Enoch, G. Tayeb, P. Sabouroux, N. Guerin, and P. Vincent, "A metamaterial for directive emission," *Physical Review Letters*, vol. 89, no. 21, p. 213902:1~4, 2002.

[5] R.Zhou, H.Zhang, HXin, 'Metallic Wire Array as Low-Effective Index of Refraction Medium for Directive Antenna Application', *Antennas and Propagation*, *IEEE Transactions* on 58 (1), 79-87, 2010.

[7] Z. Weng, N.Wang, Y. Jiao, 'Study on High Gain Patch Antenna with Metamaterial Cover', *7th International Symposium on Antennas Propagation & EM Theory*, 2006.

[6] H.Li, 'Directive Metamaterial antenna using high impedance surface', *4th Intemational Conference on Microwave and Millimeter Wave Technology Proceedings*, 2004.

[8] H.H.Soon, 'Design and Analysis of Metamaterial Antenna for Mobile Handset Application', *Antennas and Propagation*. *EuCAP*. 3rd European Conference on 2009

[9] M.L.Loughborough,'Metamaterial Loaded on Horn Antennas For DVB-T Application', *Antennas & Propagation Conference*, 2011.

[10] Y.L. Lv1,' A Zero Index Metamaterial Lens for Gain Enhancement of Patch Antenna and H-plane Horn Antenna*', Wireless Symposium (IWS),* IEEE International, 2013.

[11] C. P. Scarborough, 'Demonstration of an Octave-Bandwidth Negligible-Loss Metamaterial Horn Antenna for Satellite Applications ', *Antennas and Propagation*, IEEE Transactions on (Volume: 61, Issue: 3), 2013.

[12] D. Correia and J.M.Tin, 'Theoretical Analysis of Left-Handed Metamaterials Using FDTD-PML Method', *Microwave and Optoelectronics Conference, IMOC* 2003..

[13] R.W.Ziolkowski, 'Pulsed and CW Gaussian beam interactions with double negative metamaterial slabs', *Physical Review Letter*, 2003.

[14] Dennis M. Sullivan 'A Simplified PML for Use with the FDTD Method', *IEEE microwave and guided wave letters*, vol. 6, no. 2, february 1996.

[15] Sullivan, (2000, August) '*Electromagnetics simulations using the FDTD method'*. IEEE press series on RF and Microwave technology.

[16] J.P Berenger ,'A perfectly matched layer for the absorption of electromagnetic waves', *Journal of computational physics*, 114-185-200, 1993.